ARTICLE NO. 79-1503R

J80-205 ~~204~~

Trailing-Edge Flows at High Reynolds Number

20007
20016
20018

P. R. Viswanath,* J. W. Cleary,† H. L. Seegmiller, ‡ and C. C. Horstman §
NASA Ames Research Center, Moffett Field, Calif.

An investigation of trailing-edge flows at high Reynolds number and subsonic Mach numbers is presented. Symmetric and asymmetric trailing-edge flows are studied, each flow having pressure gradient regions upstream of the trailing edge similar to an airfoil. Measurements include model surface pressures, mean velocity, turbulent shear stress, and turbulent kinetic energy profiles in the trailing-edge and near-wake regions. Comparisons of the symmetic flow data with numerical solutions of boundary-layer as well as Navier-Stokes equations employing two different turbulence models show increasing effects of viscous interactions as the Mach number increases. Both turbulence models yielded solutions of the mean flow of comparable quality. The experimental results of the asymmetric case show the following main features: 1) in the near wake the mean flow development is significant only in the upper part of the flow; and 2) eddy viscosity concept for modeling shear stress could be applicable.

Nomenclature

k	= kinetic energy of turbulence
L	= model length
M	= Mach number
p	= static pressure
P	= total pressure
Re	= unit Reynolds number per meter
T	= temperature
u	= velocity component in x direction
u^+	= law-of-the-wall velocity coordinate, $u/\sqrt{\tau_w/\rho_w}$
$\langle u'^2 \rangle$	= mean square of velocity fluctuation in x direction
$\langle v'^2 \rangle$	= mean square of velocity fluctuation in y direction
$\langle w'^2 \rangle$	= mean square of velocity fluctuation in z direction
x	= streamwise coordinate parallel to model centerline measured from model trailing edge
y	= vertical coordinate normal to model centerline measured from the model surface and in the wake from the model trailing edge
y^+	= law-of-the-wall distance coordinate, $y\sqrt{\tau_w\rho/\mu}$
α	= flap deflection angle
δ	= boundary-layer thickness
δ^*	= displacement thickness
θ	= momentum thickness
μ	= molecular viscosity
ρ	= density
τ	= shear stress

Subscripts

L	= based on model length
n	= nominal freestream conditions
0	= reference conditions
t	= turbulent
T	= total
w	= wall

Presented as Paper 79-1503 at the AIAA 12th Fluid and Plasma Dynamics Conference, Williamsburg, Va., July 23-25, 1979; submitted Aug. 13, 1979; revision received Dec. 18, 1979. This paper is declared a work of the U. S. Government and therefore is in the public domain.

Index categories: Jets, Wakes, and Viscid-Inviscid Flow Interactions; Subsonic Flow; Transonic Flow.

*NRC Research Associate. Member AIAA.
†Research Scientist Member AIAA.
‡Research Scientist.
§Assistant Chief, Experimental Fluid Dynamics Branch. Associate Fellow AIAA.

Introduction

THE flow near the trailing edge of an airfoil and in the near wake plays an important role in airfoil design. It controls the circulation around the airfoil, and influences the entire flowfield. Trailing-edge flows can be dominated by viscous-inviscid interactions,[1] and the overall effects depend greatly on the severity of adverse pressure gradients over the rear portion of an airfoil. At Reynolds numbers of practical interest, the flow in the shear layers is generally turbulent. Predictions of boundary-layer integral thickness parameters in the trailing-edge and near-wake regions of accuracy sufficient for engineering purposes are possible[1] for moderate adverse pressure gradients when the flow remains attached to the trailing edge. However, if the adverse pressure gradients are large, as on rear-loaded airfoils at transonic speeds or on airfoils at even moderate incidence, there is a rapid thickening of the boundary layer towards the trailing edge leading to strong viscous-inviscid interactions, and our ability to predict these flows is far from satisfactory.[2,3] The difficulties are often attributed to inadequacies of boundary-layer approximations and/or turbulence modeling.[2] The airfoil flowfield, under these conditions, is generally complex involving nonequilibrium turbulent boundary layers, asymmetric merging of shear layers, and streamline curvature. Some advancement in analyzing viscous interactions with turbulent boundary layers at a trailing edge for cusped or near cusped airfoils has been successfully carried out recently by Melnik and Chow[4] and Melnik et al.[5]

From the few available studies on the subject, it is not clear whether turbulence modeling is critical in the trailing-edge region when unseparated boundary-layer conditions exist. In fact, in Ref. 1, inviscid approximations are discussed to model the flow near a trailing edge. Progress in turbulence modeling has always relied heavily on detailed experiments involving turbulence measurements. As far as trailing-edge flows are concerned, experimental data on turbulent quantities are available only for wakes of flat plates and cascades of airfoils.[6-8] Recently, Andreopoulos[7] has made a detailed experimental study of both symmetric and asymmetric near wakes of a flat plate at low speeds with a view to understand the basic mechanisms involved in interacting shear layers at a trailing edge. His measurements include conventional turbulent quantities as well as conditionally sampled data. Apart from these few basic studies, there is hardly any information on turbulence quantities on trailing-edge flows relevant to practical application. It is the main objective of the present work to improve our general understanding and prediction of trailing-edge flows in realistic flow situations and, in par-

ticular, to assess the importance of turbulence modeling aspects.

With a view toward achieving the above objective, a study of two-dimensional trailing-edge flows has been initiated at Ames. Under this program, it is planned to systematically study relatively simple trailing-edge flows of increasing complexity to aid in the better understanding of the different aforementioned effects. In this paper, new results are presented for mean velocity and turbulence quantities in the trailing-edge and near-wake regions for two different symmetric flows and an asymmetric flow at high Reynolds number and at subsonic Mach numbers. These flows have a region of pressure gradient upstream of the trailing edge (induced by the model configuration) similar to an airfoil and are attached to the trailing edge. These experiments on the symmetric cases provide a logical extension of earlier studies of flat plate near wakes[6,7] and further include compressibility effects. Comparison of the present symmetric data with numerical solutions of boundary layer as well as Navier-Stokes equations employing two different turbulent models are made. New results for the asymmetric case will provide a data base for guiding turbulence modeling as well as for comparison with asymmetric trailing-edge flow predictions.

Experiments

Experimental Arrangement and Test Conditions

The experiments were conducted in the 38.1 × 25.4 cm Ames High Reynolds Channel blowdown facility (Fig. la). The model configuration spans the test section and is made up of two parts: 1) a forebody, which is a flat plate 56.75 cm long and 2.54 cm thick with a 24.51-cm tapered forward section having a rounded leading edge (Fig. 1b); and 2) an aft body flap with a sharp trailing edge 11.63 cm long and with an included angle of 12.5 deg (Fig. 1b). The flap can be deflected to any angle within ±20 deg about the centerline. The Mach number in the test section is varied by choking the flow far downstream (see Fig. 1a). The above model configuration has been chosen in view of the following advantages: 1) it provides a thick and fully developed turbulent boundary layer desirable for modeling studies; 2) the flap can be deflected to impose different pressure gradients on the boundary layer on the flap; and 3) the relatively long length of the model combined with the high-stagnation pressures available with the facility gives high Reynolds numbers, a unique feature of the present experiments.

The test on the symmetric trailing-edge flows were conducted at two nominal freestream Mach numbers M_n of 0.4 and 0.7, while the asymmetric case was studied only at $M_n = 0.4$. The freestream Reynolds number based on model length Re_L was parametrically varied between 9×10^6 and 60×10^6 over the range of Mach numbers and stagnation pressures (P_T) of the test. Because the influence of Reynolds number on model surface pressures was found to be small, all the detailed flowfield measurements were made only at the moderately high stagnation pressure of 275×10^3 N/m^2. The values of Re_L corresponding to the above value of P_T and a nominal total temperature of 480° R are 24.3×10^6 and 36.6×10^6 at $M_n = 0.4$ and 0.7, respectively.

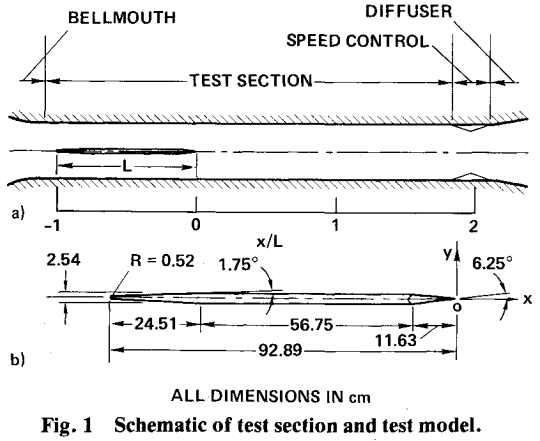

Fig. 1 Schematic of test section and test model.

Surface and Flowfield Measurements

The flat plate model described previously had 68 static pressure orifices of 0.075 cm i.d. located mostly on the centerline of the model on both upper and lower surfaces. Spanwise static pressure orifices, in the flat plate and flap region, corresponding to specific streamwise stations on the centerline were also provided to assess spanwise uniformity of surface pressures. Static pressure orifices at intervals of 10 cm were also provided on the tunnel top and bottom walls in the region of the model as well as downstream up to a distance of 45 cm. The pressures were measured with strain gage pressure transducers and each transducer was calibrated before each tunnel run.

Flowfield measurements were made using a two-color laser Doppler velocimeter (LDV) as well as conventional pitot and static probes. Two static pressure probes, one with an ellipsoidal and the other with a conical nose were employed in this study with appropriate calibrations for each probe. Pitot and static probe pressures were measured by Statham pressure transducers. Details of the LDV optical arrangement, data acquisition and processing are described in Refs. 9 and 10.

In addition to the above, the flow was visualized using spark shadowgraph technique and the surface flow on the model was examined using an oil-flow technique; a mixture of titanium dioxide and vacuum pump oil was employed for this purpose.

Two-Dimensionality of the Flowfield

Two-dimensionality was validated after making the following observations: 1) spanwise measurements of static pressure on the flat plate and flap over the central 20 cm of span that showed negligible variation about centerline value, 2) surface flow visualization using the oil-flow technique showed surface streamlines nearly parallel to the main stream direction over 90% of the span; and 3) momentum thicknesses in the symmetric wake calculated from the measured velocity profiles indicated a negligible variation in the wake region where the streamwise presure gradients are very small.

Analysis

Computations for the symmetric trailing-edge cases corresponding to experimental flow conditions have been performed using both the boundary-layer equations (BLE) and the time-dependent, mass-averaged Navier-Stokes equations (NSE). Two turbulence models were employed, the two-layer algebraic eddy-viscosity model developed by Cebeci and Smith[11] and the Wilcox-Rubesin two-equation eddy-viscosity model recently developed for compressible flow.[12]

Boundary-Layer Equation Solutions

Two boundary-layer computer codes were employed to solve the experimental flowfields with the trailing-edge flap at zero angle of attack. The algebraic eddy-viscosity model computations were made with the boundary-layer program originally described by Marvin and Sheaffer[13] and later modified by them to account for turbulent flow using the Cebeci-Smith turbulence model. On the plate the computations were carried out with the pressure gradient correction of the Van Driest damping constant. In the wake the outer-layer model was used throughout the flowfield. The two-equation eddy-viscosity model computations were made with the boundary-layer program developed by Wilcox and Traci[14] using the Wilcox-Rubesin two-equation turbulence model. In the wake no modifications were made to the turbulence model except for the use of symmetric boundary

conditions at the wake centerline. In the flow direction the grid spacing varied from 0.001% of the viscous layer thickness near the trailing edge to 25% far upstream and downstream. In the transverse direction the boundary-layer code employing the algebraic model used 51 grid points and the code employing the two-equation model used 260 points.

The computations for each turbulence model were started with a zero-pressure gradient equilibrium solution at the first measurement station ($x = -20.48$ cm) that matched the measured displacement thickness. The measured pressure distributions on the plate and at the wake centerline were used to calculate the boundary-layer edge conditions for each flowfield.

Navier-Stokes Equations Solutions

The differential equations to describe the mean flowfields are the time-dependent, mass-averaged Navier-Stokes equations for two-dimensional flow of a compressible fluid. The resulting equations are described in Ref. 15. As stated earlier, solutions to the Navier-Stokes equations were obtained using both the Cebeci-Smith algebraic and Wilcox-Rubesin two-equation turbulence models. The equations for these models are also described in Ref. 15.

Numerical Method

The numerical procedure used here is the basic explicit second-order, predictor-corrector, finite-difference, time-splitting method of MacCormack[16] modified by the efficient explicit-implicit-characteristic algorithm of Ref. 17. A description of the method used, along with its adaptation to multiequation turbulence model equations, is contained in Refs. 15 and 18. Also contained in Refs. 15 and 18 is a description of the boundary conditions and special procedures used for the turbulence model variables and equations.

Computational Domain

The computational domain is divided into a two-mesh system. Normal to the flow direction an exponentially stretched fine mesh is used to resolve that part of the flow, where viscous effects are important; the outer flow, that is predominantly inviscid, is described using a uniform coarse mesh. In the flow direction a variable mesh spacing was used concentrating most of the points close to the trailing-edge flap and in the near wake. The number of mesh points and the minimum spacing used varied with the flowfield and the turbulence model. The distance of the first y mesh point from the model wall is selected small enough so that the solutions are independent of the spacing. For the algebraic model the first mesh point off the model is taken within the viscous sublayer (typically within $y^+_{\min} \equiv y\sqrt{\tau_w \rho_w}/\mu_w < 4$); for the two-equation model, the minimum y^+ required was smaller by a factor of 10 to 20. Typical mesh sizes were 60 points in the streamwise direction and 50 points normal to the model (with 30 to 35 points in the viscous layer). In each problem, transition from the exponentially stretched fine mesh to coarse mesh occurs near the outer edge of the viscous layer. In the flow direction the mesh spacing varied from 10% of the viscous layer thickness near the trailing edge to four times the viscous layer thickness far upstream and downstream.

Boundary Conditions

The boundaries of the computational mesh extended in the vertical direction from the model surface or wake centerline to the wind tunnel wall and in the flow direction from $x = -50$ to $x = 50$ cm. The upstream boundary conditions were prescribed by a combination of uniform freestream conditions and the boundary-layer codes described above. As mentioned above, the boundary-layer computations were started with a flat-plate solution that matched the measured displacement thickness at the first measurement station for each case. The downstream boundary is positioned far enough aft of the trailing edge that all of the gradients in the flow direction can be set to zero. This boundary condition was verified by moving the location of this downstream boundary and observing substantially unchanged numerical results. The model surface is impermeable, and no-slip boundary conditions are applied with a constant wall temperature. Additional details concerning the boundary conditions for the two-equation model surface are discussed in Ref. 15. On the wake centerline symmetry conditions are imposed. At the upper boundary (the wind-tunnel wall) inviscid solid-wall boundary conditions are used. Details concerning this procedure are contained in Ref. 19.

Results and Discussion

Symmetric Case

Two symmetric flows at freestream Mach numbers of 0.4 and 0.7 have been studied. In this paper, the results at the higher Mach number are discussed in detail, while only some results at the lower Mach number are included. Additional results at $M_n = 0.4$ and a discussion of flow symmetry are all contained in Ref. 9. The experimental results are discussed first followed by comparison with numerical solutions.

Experimental Observations

The measured mean velocity profiles on the flat plate at a station 20.48 cm upstream of the trailing edge showed good agreement with the law of the wall at both Mach numbers indicating a fully developed turbulent boundary layer ahead of the flap.[9]

Model static pressure distributions normalized by the tunnel total pressure P_T are shown in Fig. 2a at both Mach numbers. The wake centerline pressures, as measured by the static pressure probes, are also included. These distributions indicate that the local freestream velocity is essentially constant over a large part of the flat plate; it accelerates near the hinge line and then decelerates over the flap in a manner similar to that over an airfoil. The sudden decrease in the wall pressure at the intersection of the flat plate and the flap is due to a rapid change in the surface curvature. The magnitude of the adverse pressure gradient on the flap increases with Mach number. There is a weak favorable pressure gradient in the near-wake region. Static pressure variations across the wake centerline were small at both Mach numbers. Figure 2b shows the static pressure distributions for the asymmetric case that will be discussed later.

For the symmetric case, the data and computational results are normalized by appropriate measured values at the edge of the boundary layer close to the trailing edge ($x = -0.4$ cm) at each Mach number M_n. For the asymmetric case, the data have been normalized by the boundary-layer edge conditions on the flat plate ($x = -40$ cm) on the upper surface. The values used are given in Table 1.

Mean velocity profiles in the trailing-edge and near-wake regions for the symmetric case at both Mach numbers are shown in Figs. 3 and 4 (note the shifted origins). As may be

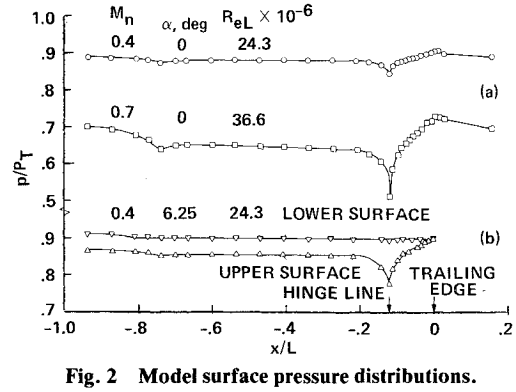

Fig. 2 Model surface pressure distributions.

Table 1 Reference values for normalizing data

M_n	u_0, m/s	$(\rho u^2)_0$ N/m^2	α, deg	δ_0^* cm	θ_0, cm
0.4	124.2	5.163×10^4	0	0.23	0.147
0.7	215.8	13.375×10^4	0	0.363	0.195
0.4	153.6	7.592×10^4	6.25		

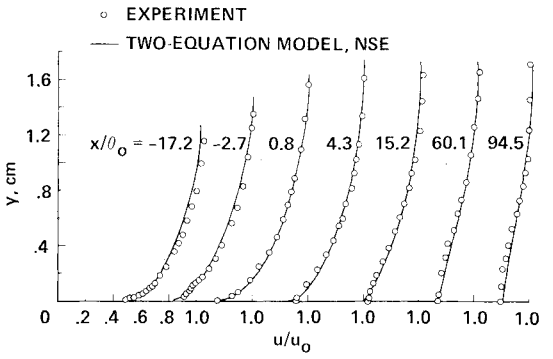

Fig. 3 Comparison of mean velocity profile measurements with computations; $M_n = 0.4$, $Re_L = 24.3\times10^6$, $\alpha = 0$ deg.

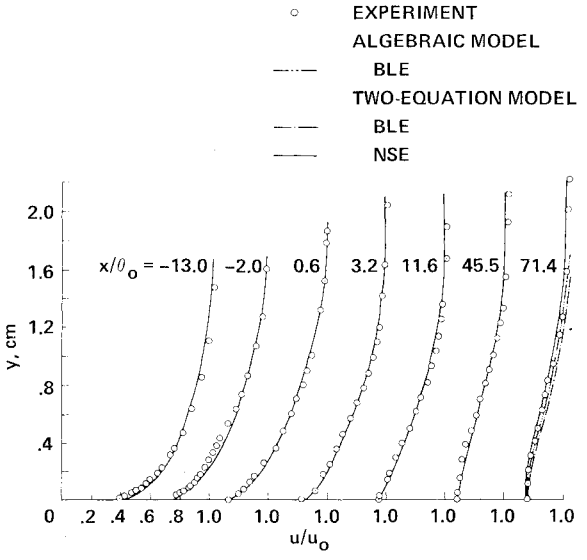

Fig. 4 Comparison of mean velocity profile measurements with computations; $M_n = 0.7$, $Re_L = 36.6\times10^6$, $\alpha = 0$ deg.

seen, measurements have been made at stations extremely close to the trailing edge. Only one-half of the symmetric wake is shown. The negative and positive values of x/θ_0 correspond to streamwise distances upstream and downstream of the trailing edge, respectively. The velocity profiles near the wall upstream of the trailing edge are less full at $M_n = 0.7$ compared to $M_n = 0.4$ indicating the effect of the increased adverse pressure gradient. The wake profiles show that in the inner region the velocities change quite rapidly with x/θ_0, while in the outer part the changes are very small at both Mach numbers. Similar observations have also been made by Andreopoulos[7] on flat-plate symmetric near wakes. The numerical solutions in Figs. 3 and 4 will be discussed later.

Figure 5 displays the streamwise variation of turbulent shear stress profiles at $M_n = 0.7$. The maximum value of the shear stress shows an increase towards the trailing edge continuing downstream in the near wake to about 3.2 θ_0. It then gradually decreases as the flow progresses downstream. The increase in shear stress ahead of the trailing edge is probably the result of the large adverse pressure gradients on

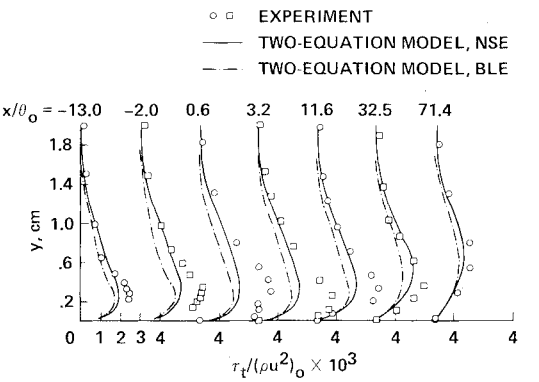

Fig. 5 Comparison of measured turbulent shear stress profiles with computations; $M_n = 0.7$, $Re_L = 36.6\times10^6$, $\alpha = 0$ deg.

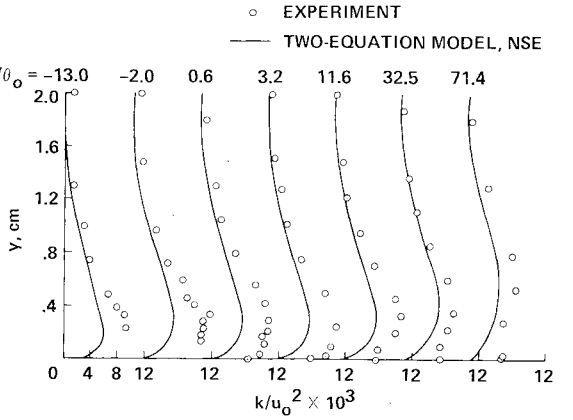

Fig. 6 Comparison of measured turbulent kinetic energy profiles with computations; $M_n = 0.7$, $Re_L = 36.6\times10^6$, $\alpha = 0$ deg.

the flap. As the wake develops, the location of the maximum shear stress moves outward. In the outer part of the wake, the normal shear stress gradients are small and there is little change in the stress in the streamwise direction. The flow in the outer region is behaving like an inviscid rotational flow.

The streamwise variation of turbulent kinetic energy profiles at $M_n = 0.7$ are shown in Fig. 6. To obtain the total value of k, the contribution from $\langle w'^2 \rangle$ was assumed equal to $\frac{1}{2}[\langle u'^2 \rangle + \langle v'^2 \rangle]$. There is a small kinetic energy increase in the inner region across the trailing edge and decreases gradually downstream. The location of the maximum kinetic energy moves away from the centerline with increasing x in a manner similar to the shear stress. On the centerline, the kinetic energy has a value comparable to the profile maximum. The centerline value decreases very slowly with streamwise distance. As with the shear stress, the kinetic energy in outer layers show little change with x. Qualitatively similar results were observed at $M_n = 0.4$ (Ref. 9.)

Comparisons with Numerical Solutions

As stated earlier, the symmetric flows have been computed using both boundary-layer as well as Navier-Stokes equations employing two different eddy-viscosity models.

Figure 7 shows predictions of model surface pressures and wall shear stress (normalized by the wall stress at $x = -20$ cm) using the Navier-Stokes equations and the two-equation Wilcox-Rubesin turbulence model. The agreement with measured surface pressures is excellent at both Mach numbers. The computed wall shear stress variations are similar at both Mach numbers; as to be expected, τ_w increases in the acceleration region near the hinge line and decreases on the flap due to the adverse pressure gradient. The surface pressure predictions using the algebraic model with the Navier-Stokes

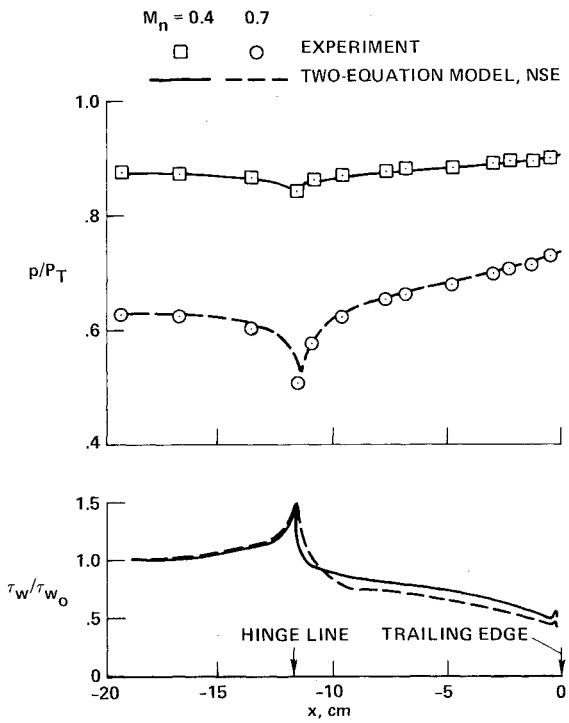

Fig. 7 Experimental and computed surface pressure measurements and computed wall shear stress variation; $\alpha = 0$ deg.

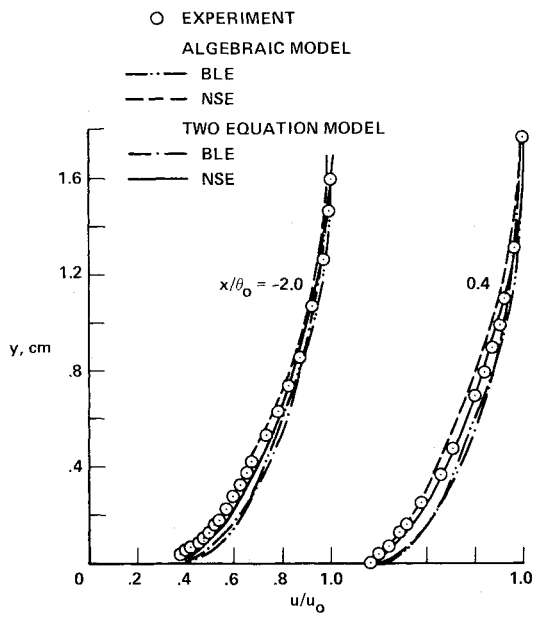

Fig. 8 Comparison of measured mean velocity profiles with different computations; $M_n = 0.7$, $Re_L = 36.6 \times 10^6$, $\alpha = 0$ deg.

equations were similar to those with the two-equation model, and hence are not shown in Fig. 7.

The computed mean velocities using both turbulence models with the Navier-Stokes as well as the boundary-layer equations are compared with data in Fig. 8, for $M_n = 0.7$. The data correspond to two streamwise stations very close to the trailing edge. Both eddy-viscosity models are adequate to compute mean velocity profiles of comparable quality. (However, the turbulent shear stress distributions of the algebraic model did not exhibit as smooth a variation with y in the trailing-edge region as the two-equation model.) The Navier-Stokes solutions show better agreement with experiment than the boundary-layer solutions regardless of the turbulence model used. This difference is a consequence of

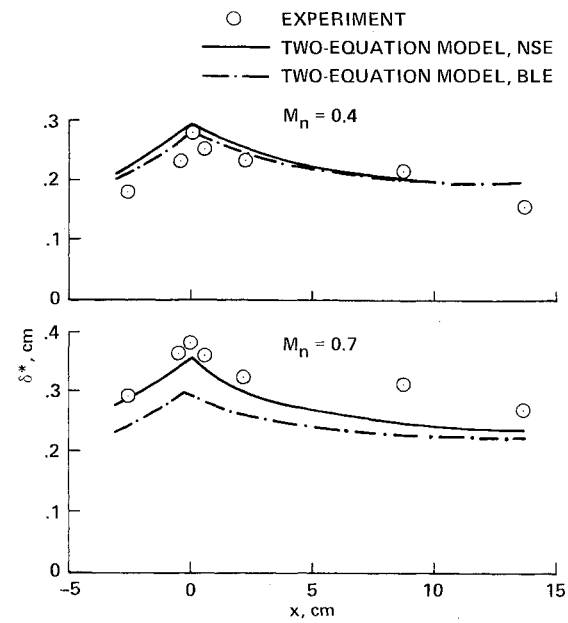

Fig. 9 Experimental and computed displacement thickness variation; $\alpha = 0$ deg.

including viscous-inviscid interaction effects near the trailing edge. A similar comparison at $M_n = 0.4$ showed that the viscous-inviscid interaction effects are not as pronounced as at $M_n = 0.7$. Most subsequent comparisons with the data will be made only with the solution of the Navier-Stokes equations employing the two-equation model.

In Figs. 3 and 4, the mean velocities obtained from the computations are also included. Good agreement is seen at both Mach numbers. At large downstream distances ($x/\theta_0 \sim 71.4$), all the different prediction methods give good agreement with data (Fig. 4).

The computed results for the turbulent shear stress and kinetic energy in the trailing-edge region are compared with the data at $M_n = 0.7$ in Figs. 5 and 6, respectively. The predictions of shear stress in the inner regions are not good except for large distances downstream ($x/\theta_0 \gtrsim 32.5$). The results from boundary-layer equations using the two-equation model are also included for comparison in Fig. 5. As to be expected, the results from Navier-Stokes equations are reatively better. As regards to turbulent kinetic energy profiles, the two-equation model shows good qualitative behavior, but underpredicts the magnitudes. Similar comparisons of turbulent shear stress and kinetic energy at $M_n = 0.4$ showed relatively better agreement with the data than at $M_n = 0.7$.[9]

The good predictions of mean velocities using the Navier-Stokes equations at $M_n = 0.7$, in spite of noticeable departures in the prediction of turbulent shear stress and kinetic energy, suggest that detailed turbulence modeling is not as important as including the effects of viscous interactions in the trailing-edge region. The comparisons shown in Fig. 8 also indicate that the first-order boundary-layer equations using the measured surface pressures do not account for all the viscous-inviscid interaction effects.

Estimate of boundary-layer displacement thickness distributions in the trailing-edge and near wake regions is important from the point of view of accounting for viscous effects. Computed results from the Navier-Stokes as well as boundary-layer equations using the two-equation model are compared with the data in Fig. 9 at both Mach numbers. At $M_n = 0.4$, where the viscous interactions are relatively weak, both predictions are nearly the same and show good agreement with the data except for some departures upstream of the trailing edge. At $M_n = 0.7$, on the other hand, where the viscous interaction effects are significant, predictions using

Navier-Stokes equations are appreciably better than the boundary-layer solutions which is consistent with the improved mean velocity predictions (Fig. 8).

Asymmetric Case

There has been growing interest in recent years concerning the study of asymmetric near-wakes.[7,8,20-22] These flows are much less understood compared to the symmetric case and the need for experimental data, particularly on turbulent quantities, to improve predictions is quite clear for the studies of Huffman and Ng[21] and Deiwert.[22] The present experiments are aimed at providing such data, for a not too complex, asymmetric flow configuration.

The experiments are made at a freestream Mach number of 0.4 and at $Re_L = 24.3 \times 10^6$. The flap is deflected downwards by an angle of 6.25 deg so that the lower surface of the flap is in line with the lower surface of the flat plate, providing a zero-pressure gradient turbulent boundary-layer flow on the lower surface. This configuration is of particular interest from the point of view of general understanding as well as modeling since only the turbulent boundary layer on the upper surface experiences a pressure gradient.

Experimental Observations

Figure 2b shows the model static pressure distributions. As may be seen, there is a circulation developed around the model, and the static pressures on the flat plate on the upper and lower surfaces are practically constant at different levels; the corresponding Mach numbers are 0.48 and 0.39, respectively. On the upper surface, the flow accelerates towards the hinge line and decelerates on the flap.

Mean velocity profiles in the trailing-edge and near-wake regions for both sides of the flow are shown in Fig. 10. In this figure, as well as in some of the subsequent ones, lines have been faired through the data for clarity. Upstream of the trailing edge, the profile on the upper surface is thicker and less full compared to that on the lower surface reflecting the effect of an adverse pressure gradient.

The streamwise development of mean velocity in the near wake is best seen in Fig. 11. In regard to the upper part of the near wake, changes all across the width can be seen but are more pronounced in the inner regions. This is in contrast to the symmetric case discussed earlier. In the lower part, on the other hand, changes are seen only in a narrow region around $y = 0$, and a large part of the profile shows no change. The

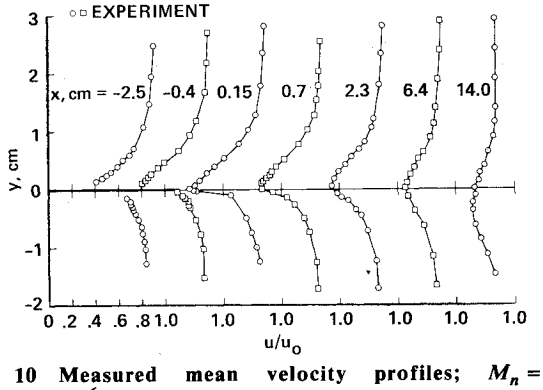

Fig. 10 Measured mean velocity profiles; $M_n = 0.4$. $Re_L = 24.3 \times 10^6$, $\alpha = 6.25$ deg.

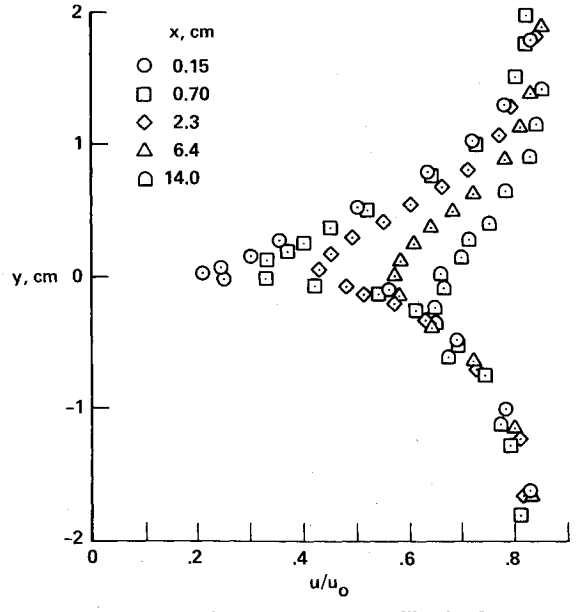

Fig. 11 Development of mean velocity profiles in the near wake, $M_n = 0.4$, $Re_L = 24.3 \times 10^6$, $\alpha = 6.25$ deg.

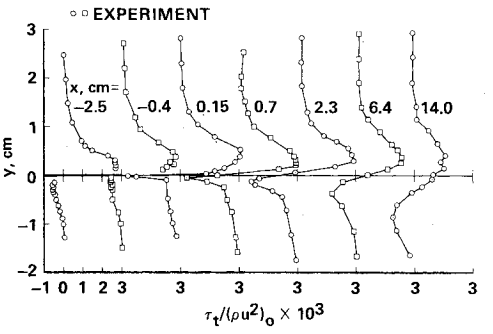

Fig. 12 Measured turbulent shear stress profiles; $M_n = 0.4$, $Re_L = 24.3 \times 10^6$, $\alpha = 6.25$ deg.

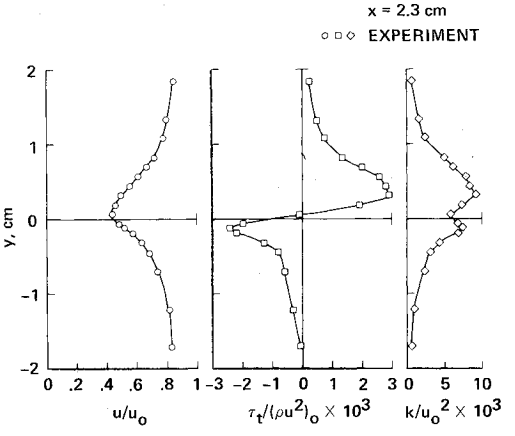

Fig. 13 Measured mean velocity, turbulent shear stress and turbulent kinetic energy profiles; $M_n = 0.4$, $Re_L = 24.3 \times 10^6$ $\alpha = 6.25$ deg.

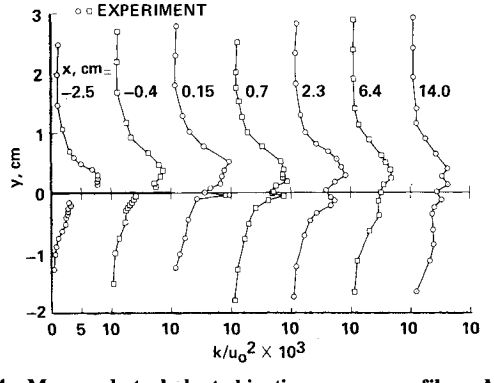

Fig. 14 Measured turbulent kinetic energy profiles; $M_n = 0.4$, $Re_L = 24.3 \times 10^6$, $\alpha = 6.25$ deg.

profile at the last measurement station ($x = 14$ cm) is still asymmetric.

Figure 12 shows the turbulent shear stress profiles. Large normal gradients in the vicinity of the minimum velocity location are seen. The data also show that the shear stress varies linearly with y in this narrow region. Further, the results show that the shear stress and velocity gradient, $\partial u/\partial y$, vanish at the same location (see Fig. 13). This implies that eddy-viscosity concept can be employed to model the stress in prediction methods. The profiles show two peaks, corresponding to the upper and lower flows. A closer examination of these profiles shows that, except in the vicinity of $y = 0$, the shear stress is nearly frozen between $x = 0.15$ and $x = 2.3$ cm, but changes are seen at $x = 6.4$ cm.

The turbulent kinetic energy profiles are displayed in Fig. 14. In the inner region, the kinetic energy increases across the trailing edge. The near wake profiles show a characteristic local minimum at the zero-velocity gradient location (see Fig. 13). As with the shear stress, two peaks are seen. Changes in the streamwise direction, except in the vicinity of minimum velocity location, are generally small for both upper and lower flows.

Computation of this flow using the Navier-Stokes equations is in progress at Ames and experimental data are also being gathered for the same configuration, but at a higher freestream Mach number.

Concluding Remarks

With a view to improving our general understanding, and in particular, to assess the importance of turbulence modeling aspects of trailing-edge flows, detailed experiments have been made at subsonic Mach numbers and at high Reynolds number representative of flight conditions. Symmetric and asymmetric trailing-edge flow configurations have been studied. All these flows have a region of adverse pressure gradient upstream of the trailing edge similar to an airfoil. Flowfield measurements of mean and turbulent quantities have been made using a laser velocimeter.

Comparisons of the symmetric flow data with numerical solutions of the boundary layer as well as Navier-Stokes equations employing two different turbulence models show increased effects of viscous interactions in the trailing-edge region as the Mach number increases. Both turbulence models yielded solutions of the mean flow of comparable quality.

The experimental results of the asymmetric case show the following features: 1) in the near wake, the mean flow development is significant in the upper part of the flow; 2) the turbulent shear stress distributions in the near wake, close to the trailing edge, are nearly frozen; and 3) eddy-viscosity concept for modeling shear stress could be applicable. In addition, the data provide a base for guiding turbulence modeling as well as for comparison with asymmetric trailing-edge flow predictions.

Acknowledgment

The authors thank M. J. Lanfranco for his assistance in performing some of the boundary-layer computations.

References

[1] Green, J. E., "Some Aspects of Viscous Inviscid Interactions at Transonic Speeds and Their Dependence on Reynolds Number," AGARD-CP-83-71, 1971.

[2] Spaid, F. W. and Hakkinen, R. J., "On the Boundary Layer Displacement Effect Near the Trailing Edge of an Aft-Loaded Airfoil," *Journal of Applied Mathematics and Physics,* Vol. 28, Sept. 1977, pp. 941-950.

[3] Lock, R. C., "The Prediction of Viscous Effects on Aerofoils in Transonic Flow," Paper for DGLR Symposium, Bad Harzburg, West Germany, June 1978.

[4] Melnik, R. E., and Chow, R., "Asymptotic Theory of Two-Dimensional Trailing-Edge Flows," NASA SP-347, 1975.

[5] Melnik, R. W., Chow, R., and Mead, H. R., "Theory of Viscous Transonic Flow over Airfoils at High Reynolds Number," AIAA Paper 77-680, 1977.

[6] Chevray, R. and Kovasznay, L. S. G., "Turbulence Measurements in the Wake of a Thin Flat Plate," *AIAA Journal,* Vol. 7, Aug. 1969, pp. 1641-1643.

[7] Andreopoulos, J., "Symmetric and Asymmetric Near Wake of a Flat Plate," Ph.D. Thesis, London University, July 1978.

[8] Raj, R. and Lakshminarayana, B., "Characteristics of the Wake Behind a Cascade of Airfoils," *Journal of Fluid Mechanics,* Vol. 61, Dec. 1973, pp. 707-730.

[9] Viswanath, P. R., Cleary, J. W., Seegmiller, H. L. and Horstman, C. C., "Trailing-Edge Flows at High Reynolds Number," AIAA Paper 79-1503, 1979.

[10] Seegmiller, H. L., Marvin, J. G. and Levy, Jr. L. L "S ady and Unsteady Transonic Flow," *AIAA Journal,* Vol. 16, De 978, pp. 1262-1270.

[11] Cebeci, T. and Smith, A. M. O., *Analysis of Turbulent Boundary Layers,* Academic Press. N. Y., 1974.

[12] Wilcox, D. C., and Rubesin, M. W., "Progress in Turbulence Modeling for Complex Flow Fields Including Effects of Compressibility," NASA TP-1517, 1979.

[13] Marvin, J. G. and Sheaffer, Y. S., "A Method for Solving the Nonsimilar Boundary-Layer Equations Including Foreign Gas Injection," NASA TN D-5516, 1969.

[14] Wilcox, D. C. and Traci, R. M., "A Complete Model of Turbulence," AIAA Paper 76-351, July 1976.

[15] Viegas, J. R. and Horstman, C. C., "Comparison of Multiequation Models for Several Shock Separated Boundary-Layer Interaction Flows," AIAA Paper 78-1165, July 1978.

[16] MacCormack, R. W., "Numerical Solution of the Interaction of a Shock Wave with a Laminar Boundary Layer," *Lecture Notes in Physics,* Vol. 8, Springer-Verlag, 1971, pp. 151-163.

[17] MacCormack, R. W., "An Efficient Numerical Method for Solving the Time-Dependent Compressible Navier-Stokes Equations at High Reynolds Number," *Computing in Applied Mechanics,* AMD Vol. 18, American Society of Mechanical Engineers, 1976.

[18] Coakley, T. J. and Viegas, J. R., "Turbulence Modeling of Shock Separated Boundary-Layer Flows," presented at the Symposium on Turbulent Shear Flows, University Park, Pa., April 1977.

[19] Levy, L. L., "Experimental and Computational Steady and Unsteady Transonic Flows About a Thick Airfoil," *AIAA Journal,* Vol. 16, June 1978, pp. 564-572.

[20] Leuchter, O., "Effect of Free-Stream Turbulence and Initial Boundary Layers on the Development of Turbulence Mixing Layers," *Project SQUID Workshop: Turbulence in Internal Flows,* edited by S. N. B. Murthy, Hemisphere Publishing Corp., June 1976.

[21] Huffman, G. D. and Ng, B. S. H., "Modeling of an Asymmetric Turbulent Near Wake Using the Interaction Hypothesis," *AIAA Journal,* Vol. 16, March 1978, pp. 193-194.

[22] Deiwert, G. S., "Computation of Turbulent Near Wake for Asymmetric Airfoils," NASA TM-78581, 1979.